Exploring Spin direction-tidal field correlations of Dark Matter haloes

Sumit Kumar Adhya
Guide: Prof. Shadab Alam

October 12, 2025

Contents

Chapter 1

Reproducing Sujatha et. al. 2019

1.1 Introduction

The goal of this section is to reproduce the main result of the paper: Tidal web anisotropy (α) is a primary indicator of halo assembly bias. We use the Sahyadri N body simulation data for our analysis. But before that we recall some key definitions from the paper which would be usefule for our analysis.

1.2 Measuring internal halo properties

All internal halo properties used in the analysis are computed using only gravitationally bound particles belonging to the FoF group of each halo. Below we summarise the definitions and notation used.

1.2.1 Mass ellipsoid tensor and shape

The mass ellipsoid (shape) tensor M_{ij} of a halo is computed by summing over bound particles following the iterative prescription of Allgood et. al. (2006):

$$M_{ij} \;=\; \sum_{n\in\text{halo}} \frac{x_{n,i}\, x_{n,j}}{r_n^2}\,, \tag{1.1}$$

where $x_{n,i}$ is the i-th component of the n-th particle position relative to the halo centre and

$$r_n^2 \;=\; x_n^2 \;+\; \frac{y_n^2}{(b/a)^2} \;+\; \frac{z_n^2}{(c/a)^2} \tag{1.2}$$

is the ellipsoidal distance used during iteration. Diagonalising M_{ij} yields ordered eigenvalues $a^2 \geq b^2 \geq c^2$. Common summary measures are:

- the minor-to-major axis ratio, c/a, with $0 \leq c/a \leq 1$; $c/a = 1$ corresponds to a sphere.
- the triaxiality parameter, $T = (a^2 - b^2)/(a^2 - c^2)$, which indicates whether the ellipsoid is prolate ($T \to 1$) or oblate ($T \to 0$).

1.2.2 Velocity ellipsoid tensor

The velocity ellipsoid tensor measures anisotropy in the halo velocity dispersion. For a halo with N particles:

$$V_{ij}^2 \;=\; \frac{1}{N} \sum_{n\in\text{halo}} \left(v_{n,i} - \langle v_i\rangle\right)\left(v_{n,j} - \langle v_j\rangle\right), \tag{1.3}$$

where $v_{n,i}$ is the i-th velocity component of the n-th particle and $\langle v_i \rangle$ is the bulk halo velocity. Diagonalising V_{ij}^2 gives eigenvalues $a_v^2 \geq b_v^2 \geq c_v^2$ and we use the ratio c_v/a_v as a measure of the velocity-ellipsoid asphericity (analogous to c/a for the mass ellipsoid).

1.2.3 Velocity anisotropy

The (global) velocity anisotropy β is defined by

$$\beta \;=\; 1 - \frac{\sigma_t^2}{2\sigma_r^2}\,, \tag{1.4}$$

where σ_r^2 and σ_t^2 are the radial and tangential velocity dispersions of halo particles (computed inside the mass ellipsoid). $\beta = 0$ corresponds to an isotropic velocity distribution; $\beta > 0$ indicates radial dominance, while $\beta < 0$ indicates tangential dominance.

1.2.4 Concentration

Halo concentration $c_{\rm vir}$ is measured by fitting the spherically averaged density profile to an NFW form,

$$\rho(r) = \frac{\rho_s}{(r/r_s)(1 + r/r_s)^2}\,, \tag{1.5}$$

and defining

$$c_{\rm vir} \equiv \frac{R_{\rm vir}}{r_s}\,, \tag{1.6}$$

where r_s is the NFW scale radius from the fit. Concentration is a commonly used proxy for formation epoch.

1.2.5 Spin

The (Peebles) dimensionless spin parameter λ is

$$\lambda \;=\; \frac{J\,|E|^{1/2}}{G\,M_{\rm vir}^{5/2}}\,, \tag{1.7}$$

where J is the halo angular momentum magnitude, E its total energy, $M_{\rm vir}$ the virial mass and G Newton's constant. Rockstar also provides the Bullock variant

$$\lambda' \;=\; \frac{J_{\rm vir}}{\sqrt{2}\,M_{\rm vir}\,R_{\rm vir}\,V_{\rm vir}} \tag{1.8}$$

which is sometimes used interchangeably; both quantify rotational support of the halo.

1.2.6 Tidal anisotropy α

Tidal anisotropy quantifies the degree to which the local tidal field around a halo is anisotropic. We follow the same definition used in the reference work and in our pipeline: the tidal tensor is evaluated at a fixed scale ($4 \times R_{200b}$ in our case) and diagonalised to obtain its eigenvalues $\lambda_1, \lambda_2, \lambda_3$ (ordered arbitrarily in the catalog). From these we construct two scalar combinations that capture the isotropic and anisotropic parts of the tidal field used throughout this work:

$$\text{trace} \;=\; \delta \;=\; \lambda_1 + \lambda_2 + \lambda_3$$

$$q^2 \;=\; \tfrac{1}{2}\Big[(\lambda_1 - \lambda_2)^2 + (\lambda_1 - \lambda_3)^2 + (\lambda_2 - \lambda_3)^2\Big]$$

The tidal anisotropy α is then defined as

$$\alpha \;=\; \frac{\sqrt{q^2}}{1+\delta}\,.$$

This form isolates the anisotropic shear (numerator) and normalises by the local isotropic compression/expansion (denominator), so α is large only when shear is substantial relative to the local density. In our implementation we compute λ_i from the columns `lam1_R4R200b`, `lam2_R4R200b` and `lam3_R4R200b` in the provided catalogue and then compute q^2, δ and α exactly as above.

1.2.7 Halo bias b_1

Halo bias describes how strongly haloes of a given population trace (or are biased relative to) the underlying matter distribution on large scales. In the analyses and plots of this report we use a halo-by-halo estimator of the large-scale linear bias, denoted b_1, provided in the halo catalogue (column `b1`). In the original reference this quantity is obtained by comparing the halo overdensity to the matter overdensity on sufficiently large scales.

1.2.8 Notes on measurement

- All of the above quantities are computed using bound particles assigned by the halo finder (rockstar), and in practice the mass ellipsoid and velocity ellipsoid calculations restrict the particle sums to the relevant ellipsoidal region.
- Iterative procedures are used where needed (mass ellipsoid determination), starting from a spherical guess and updating axis ratios until convergence.
- These scalar summaries (e.g. c/a, c_v/a_v, β, $c_{\rm vir}$, λ) are the quantities used in the assembly-bias analysis (section 3) and are compared to the tidal-anisotropy α and halo-by-halo bias b_1.

1.3 Sahyadri Simulation data

In our analysis, we use the data from the Sahyadri N-body cosmological simulation at redshift z=0. The dataset contains dark matter halo catalogs generated using the ROCKSTAR halo finder and include comprehensive halo properties across three files-basic, extended and vahc. The Basic catalog contains essential halo properties including masses, radii, positions, velocities, and basic shape parameters. The Extended catalog contains detailed halo properties including merger tree information, accretion history, spin parameters, and shape measurements and the Vahc catalog contains Velocity Anisotropy Halo Catalog (VAHC) data - custom calculations from the Sahyadri simulation measuring tidal tensor eigenvalues at different radial scales. These parameters characterize the local tidal environment around each halo.
The data we have for $z = 0$ contains information for 10549241 haloes. For our study we first convert the fits files into csv's., followed by extracting the relevant columns into a pandas dataframe.
To understand some basic features and trends followed by the haloes, we obtain the following plots.
Inference:-

1. **Halo Mass Function:** The halo mass distribution exhibits a steep decline toward higher masses. The majority of halos occupy the intermediate mass range (10^9–$10^{11}\,M_\odot/h$), while massive cluster-scale halos ($> 10^{12}\,M_\odot/h$) are comparatively rare, as expected from

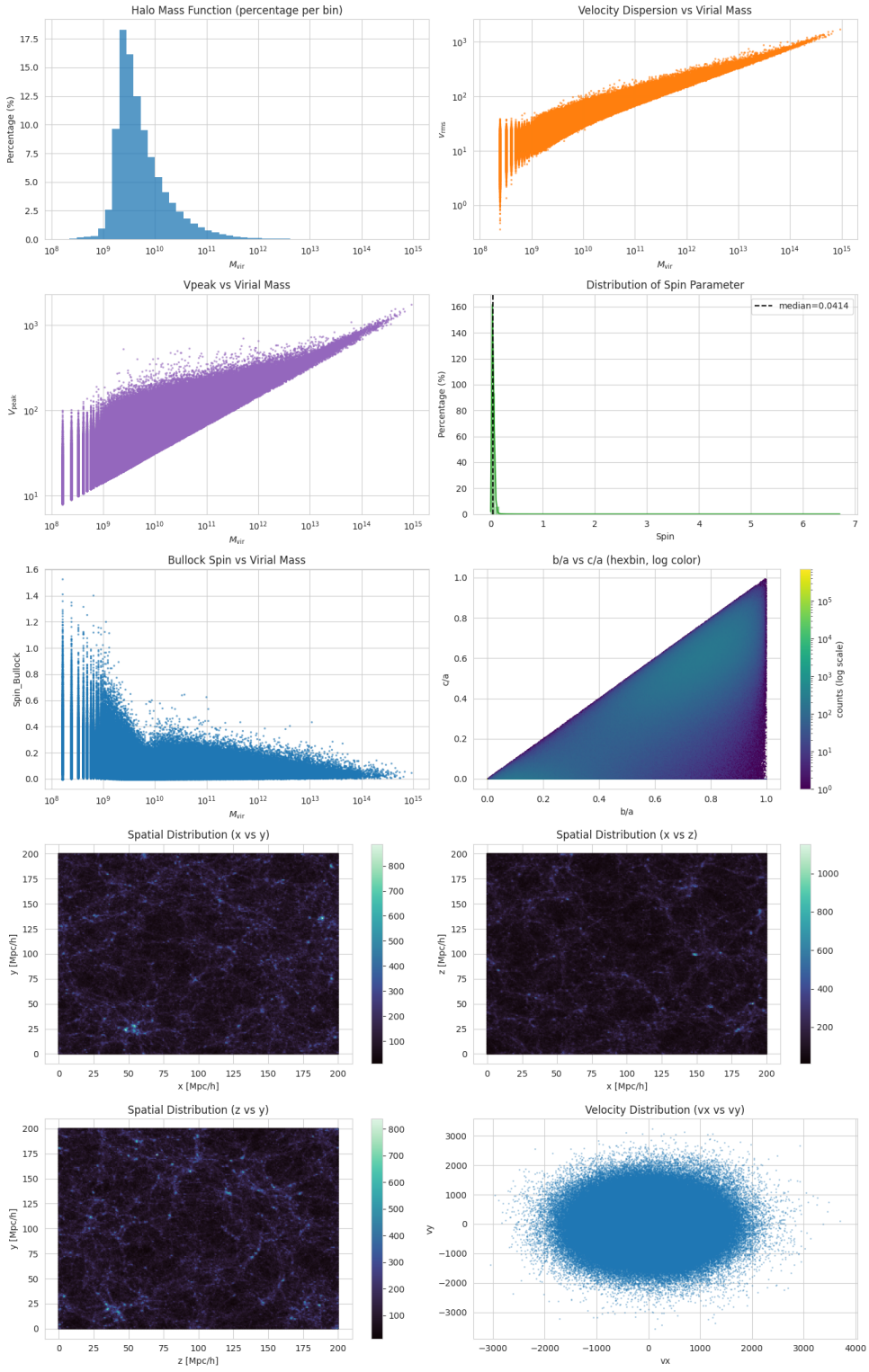

Figure 1.1:

hierarchical assembly. Larger/More massive haloes correspond to, very high overdensities in the primorial field which is rarer and statistically much less likely.

2. **Kinematic Relations ($v_{\rm rms}$ and $V_{\rm peak}$):** Both the velocity dispersion ($v_{\rm rms}$) and the peak circular velocity ($V_{\rm peak}$) scale positively with halo mass. This is very much expected because of a deeper potential well formed by higher mass haloes.

3. **Spin Parameter Distribution:** The spin parameter (λ) distribution peaks sharply at low values ($\lambda \sim 0.03$–0.05). The presence of a small high-spin tail likely corresponds to recently merged or unrelaxed halos.

4. **Spin–Mass Relation:** The Bullock spin parameter ($\lambda_{\rm Bullock}$) shows a weak inverse correlation with virial mass, indicating that low-mass halos tend to have slightly higher spins. This behavior is consistent with the tidal torque theory, where angular momentum acquisition is more efficient for smaller systems.

5. **Shape Distribution (b/a vs. c/a):** The hexbin map of axis ratios indicates that most halos are moderately triaxial, clustering around $b/a, c/a \approx 0.4$–0.8. The triangular region arises from the geometric constraint $c/a \leq b/a \leq 1$.

6. **Spatial Distribution:** The (x, y), (x, z), and (z, y) hexbin density maps reveal a filamentary large-scale structure characteristic of the cosmic web. Dense nodes connected by filaments and surrounded by underdense voids reproduce the expected morphology of dark matter distribution $z \approx 0$.

7. **Velocity Distribution:** The velocity scatter (v_x, v_y) shows a symmetric, roughly elliptical distribution centered around zero, implying isotropic velocity dispersion and the absence of large-scale bulk flows. The Gaussian-like spread supports the interpretation that halos are statistically virialized and dynamically relaxed.

1.4 Assembly Bias trends

In this section we reproduce Fig. 1 of []. We use the measurements of the halo bias and various other internal properties obtained from the simulated data .

1.4.1 Due to tidal anisotropy (α)

We compute the tidal anisotropy at $4 \times R_{200b}$ as used in the paper. We have the eigenvalues of the tidal tensor at $4 \times R_{200b}$ in the columns: "lam1_R4R200b", "lam2_R4R200b" and "lam3_R4R200b" of vahc.csv. Using these and the usual formula for α as given in the paper and discussed in the previous section we compute the tidal anisotropy (α) for each halo. We then perform logarithmic binning for the mass range and for every bin, we sort the halos in increasing order of α and make quartiles: $Q1 = 0 - 25\%$, $Q2 = 25\% - 50\%$, $Q3 = 50\% - 75\%$ and $Q4 = 75\% -$ rest with respect to the values of α. We then obtain the quartile plot of the halo bias(b_1) vs M_{vir}, the quartiles being with respect to α. The plot is obtained as shown in the figure below:

Inference: Out of the 10 bins (0-9) the results for bin 3-9 matches satisfactorily with the paper. There is some abnormality in the low mass range(bin: 0-2). To figure that out, we print the no. of halos per quartile per bin and also the min/max values for each such quartile for each bin. For bins 0-2, we observe that a large no. of halos get the same value of α (near zero) and that therefore doesn't show reliable assembly bias trends in this mass range. So we can conclude that haloes in isotropic environments (small α) are substantially less clustered(low b_1) than those in anisotropic environments (high α).

1.4.2 Due to Spin

We follow the same procedure as before with the "Spin" column of the "extended.csv" data which actually is the Peebles spin parameter as discussed in the paper as well as in the previous section. We then obtain the following plot. Again the plot agrees quite well with that in Fig. 1 in the paper.

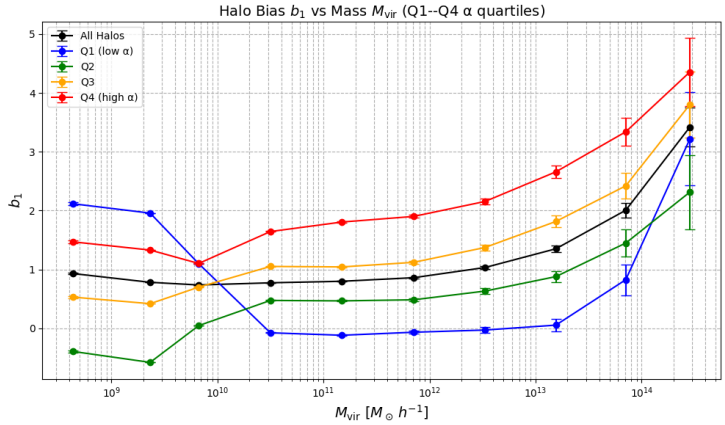

Figure 1.2: Assembly bias for α: tidal anisotropy

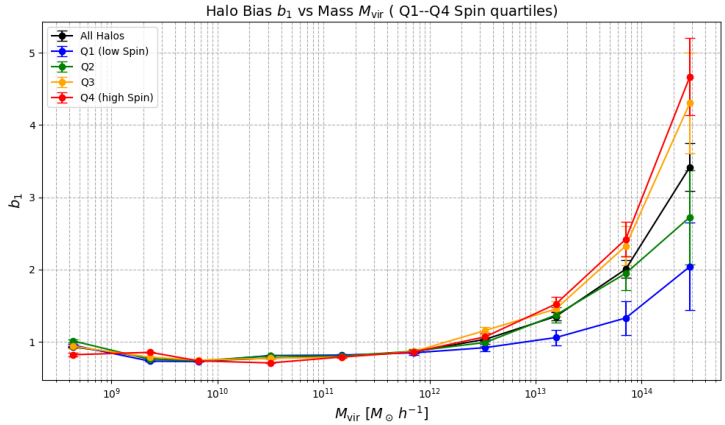

Figure 1.3: Assembly bias for λ: Peebles' Spin

Inference: We observe that the assembly bias trend is stronger for the high mass range (bins-6 7,8,9) while for lower masses (bin-0-5), the halo spin shows nearly no assembly bias. This can be explained as follows:
At early times, a halo's spin mostly comes from the tidal torques. For low mass haloes this process happens early, in relatively linear environments. Their environments are kind of isolated thus having not much connection between their spin and the large-scale environment. On the contrary, for high mass haloes, they form later through lots of mergers in denser regions. Their spin is heavily influenced by how and when they merge. Since dense regions statistically have more merger activity, spin becomes correlated with the environment thus showing high positive assembly bias. We also observe that for high mass haloes (bin 6-9), haloes with smaller spin are less clustered than those with higher spins.

1.4.3 Due to c/a

After following a similar procedure for the halo shape asphericity (c/a) using the c_to_a column of the extended.csv file, we get the following plot:
Inference: The assembly bias trend matches with that in the paper for bins 1-8, for bin 9, there aren't enough no. of haloes, and therefore not showing reliable statistics. For bin 0, we again have same value of c/a for a large number of haloes thus not showing reliable assembly bias trend.

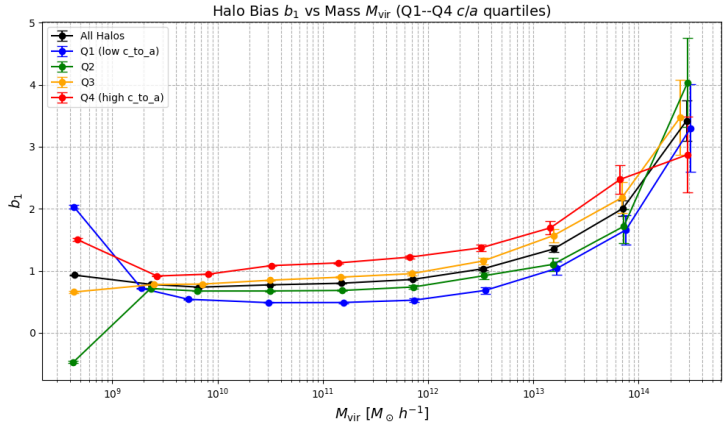

Figure 1.4: Assembly bias for c/a: Halo Shape asphericity

1.4.4 Due to c_{vir}

We compute the halo concentration(c_{vir}) for each one of the haloes and follow again the similar procedure as before to get the following quartile plot.

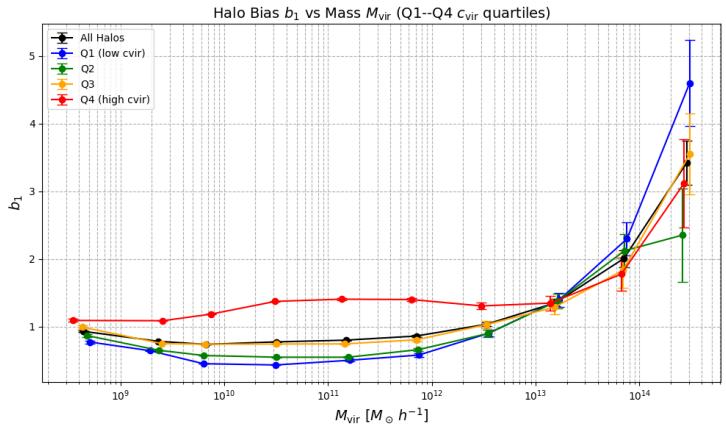

Figure 1.5: Assembly bias for c_{vir}: Halo Concentration

Inference: As similar to the paper, the assembly bias for c_{vir} shows a more complex trend. For lower masses (bins 0-7), the haloes show a positive assembly bias with respect to c_{vir}, i.e. highly concentrated haloes being more clustered. For higher masses this flips. This inversion as can be observed from the plot happens at nearly $M_{vir} \sim 10^{13} h^{-1} M_\odot$ and this matches with that reported in the paper.

1.5 Tidal Anisotropy as an indicator of assembly bias

To determine whether the tidal anisotropy (α) is an indicator or acts as an intermediate step for assembly bias, we use the concept of conditional correlation coefficients. We first apply a mass cut $M_{\rm vir} > 10^{10}\ h^{-1} M_\odot$, since low mass haloes doesn't show significant assembly bias trends as observed in the previous section. We then split the remaining haloes into 10 logarithmically spaced mass bins. We, thereafter compute the conditional correlation coefficient:

$$\gamma_{b_1,c|\alpha} \;=\; \gamma_{b_1,c} \;-\; \gamma_{b_1,\alpha}\,\gamma_{\alpha,c}, \tag{1.9}$$

where c is some internal property. We then use the same reasoning as used in the paper that if $\gamma_{b_1,c|\alpha} = 0$, then $\gamma_{b_1,c} \;=\; \gamma_{b_1,\alpha}\,\gamma_{\alpha,c}$ which implies that the b_1-property covariance is explained

by the joint correlation of both b_1 and c with α. In other words, conditioning on α removes the assembly bias trend for the internal properties. We now try to reproduce this result using our data. In this analysis we use Spearman's rank correlation. We first compute the Spearman's rank correlation between α and an internal property(left panel), which depicts the corr. between the tidal environment and the halo internal properties, next we compute the same for b_1 and an internal property(middle panel) which depicts the assembly bias of halo internal properties and at last the conditional correlation coefficients between b_1 and the internal properties, conditioned on α, which basically depicts the residual assembly bias at fixed tidal environment.

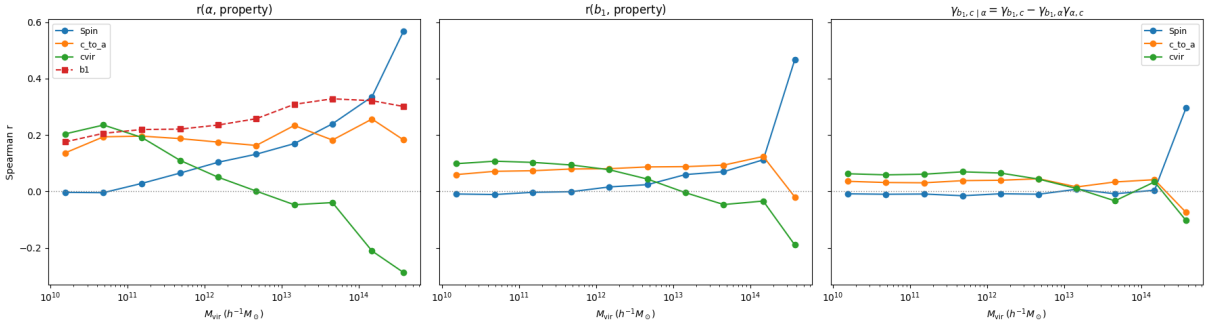

Figure 1.6: Correlations between internal halo properties, tidal environment and large scale bias

Inference: The left panel broadly matches with the paper depicting a positive correlation between the tidal environment and the clustering strength, spin and halo shape asphericity, while showing a positive correlation for lower masses and a negative correlation for higher masses with the halo concentration. The middle panel summarizes the assembly bias trends we obtained earlier. And the right panel depicts the result of the paper that the conditional correlation coefficients (although not 0) significantly reduce in magnitude from the unconditional coefficients in the middle panel (only large residuals remain for higher mass haloes). This suggests that conditioning on the tidal anisotropy α largely accounts for the assembly bias trend of the internal halo properties, thus producing the main result of the paper.

Bibliography

Sujatha et. al.(2019)